Journal of Geophysical Research: Oceans

RESEARCH ARTICLE
10.1029/2018JC013982

A New Bathymetry for the Southeastern Filchner-Ronne Ice Shelf: Implications for Modern Oceanographic Processes and Glacial History

S. H. R. Rosier[1,2], C. Hofstede[3], A. M. Brisbourne[1], T. Hattermann[4,3], K. W. Nicholls[1], P. E. D. Davis[1], P. G. D. Anker[1], C.-D. Hillenbrand[1], A. M. Smith[1], and H. F. J. Corr[1]

[1]British Antarctic Survey, Cambridge, UK, [2]Now at Geography and Environmental Sciences, Northumbria University, Newcastle, UK, [3]Alfred Wegener Institute Helmholtz Centre for Polar and Marine Research, Bremerhaven, Germany, [4]Akvaplan-niva AS, Tromsø, Norway

Key Points:
- Data from a recent seismic survey of the southeastern Filchner-Ronne Ice Shelf are presented
- Together with previous measurements, a new bathymetric grid of the region is produced
- New features identified in the grid have important oceanographic and glaciological implications

Supporting Information:
- Supporting Information S1
- Figure S1
- Figure S2

Correspondence to:
S. H. R. Rosier,
sebastian.rosier@northumbria.ac.uk

Citation:
Rosier, S. H. R., Hofstede, C., Brisbourne, A. M., Hattermann, T., Nicholls, K. W., Davis, P. E. D., et al. (2018). A new bathymetry for the southeastern Filchner-Ronne Ice Shelf: Implications for modern oceanographic processes and glacial history. *Journal of Geophysical Research: Oceans*, *123*, 4610–4623. https://doi.org/10.1029/2018JC013982

Received 14 MAR 2018
Accepted 28 MAY 2018
Accepted article online 8 JUN 2018
Published online 5 JUL 2018

Abstract The Filchner-Ronne Ice Shelf, the ocean cavity beneath it, and the Weddell Sea that bounds it, form an important part of the global climate system by modulating ice discharge from the Antarctic Ice Sheet and producing cold dense water masses that feed the global thermohaline circulation. A prerequisite for modeling the ice sheet and oceanographic processes within the cavity is an accurate knowledge of the sub-ice sheet bedrock elevation, but beneath the ice shelf where airborne radar cannot penetrate, bathymetric data are sparse. This paper presents new seismic point measurements of cavity geometry from a particularly poorly sampled region south of Berkner Island that connects the Filchner and Ronne ice shelves. An updated bathymetric grid formed by combining the new data with existing data sets reveals several new features. In particular, a sill running between Berkner Island and the mainland could alter ocean circulation within the cavity and change our understanding of paleo-ice stream flow in the region. Also revealed are deep troughs near the grounding lines of Foundation and Support Force ice streams, which provide access for seawater with melting potential. Running an ocean tidal model with the new bathymetry reveals large differences in tidal current velocities, both within the new gridded region and further afield, potentially affecting sub-ice shelf melt rates.

Plain Language Summary The Filchner-Ronne Ice Shelf in Antarctica is the largest body of floating ice in the world and plays an important role in the global climate system through its interactions with the ocean and Antarctic Ice Sheet. Due to its thickness and remoteness, the shape of the large ocean cavity beneath this floating ice shelf is poorly understood, yet this information is crucial for ice and ocean models of the region. In this study we present recent measurements of the thickness of this ocean cavity and, in combination with previous measurements, produce a new map of the area. A number of new features are revealed in this map, and we discuss the implications for ocean currents within the cavity, as well as past and future ice sheet flow.

1. Introduction

Ice discharge from the Antarctic Ice Sheet (AIS) occurs primarily through ice shelves by iceberg calving and basal melting (Rignot et al., 2013). Ice shelf thinning can lead to a reduction in the buttressing effect that the ice shelf can exert on grounded ice, thereby increasing ice discharge across the grounding line and into the ocean (Hughes, 1973; Thomas, 1973). The recent breakup of small ice shelves on the Antarctic Peninsula has led to an increase in ice flux from these areas (Dupont & Alley, 2005; Rott et al., 2002; Scambos et al., 2004), prompting the suggestion that the thinning or breakup of much larger ice shelves could result in considerable sea level rise (Payne et al., 2004; Reese et al., 2018). Interactions with the ocean at the base of the ice shelves—melting and refreezing—therefore have consequences for both ice sheet stability and ocean circulation. In these ways, the floating ice shelves that surround much of the Antarctic continent play an important role in the global climate system.

The Filchner-Ronne Ice Shelf (FRIS) is by volume the largest body of floating ice in the world (Fox et al., 1994) and accounts for ~11% of ice discharge from the AIS (Gardner et al., 2018). It is flanked to the north by the Weddell Sea, which is the source of about 40% of Antarctic bottom water (Meredith, 2013), making this region

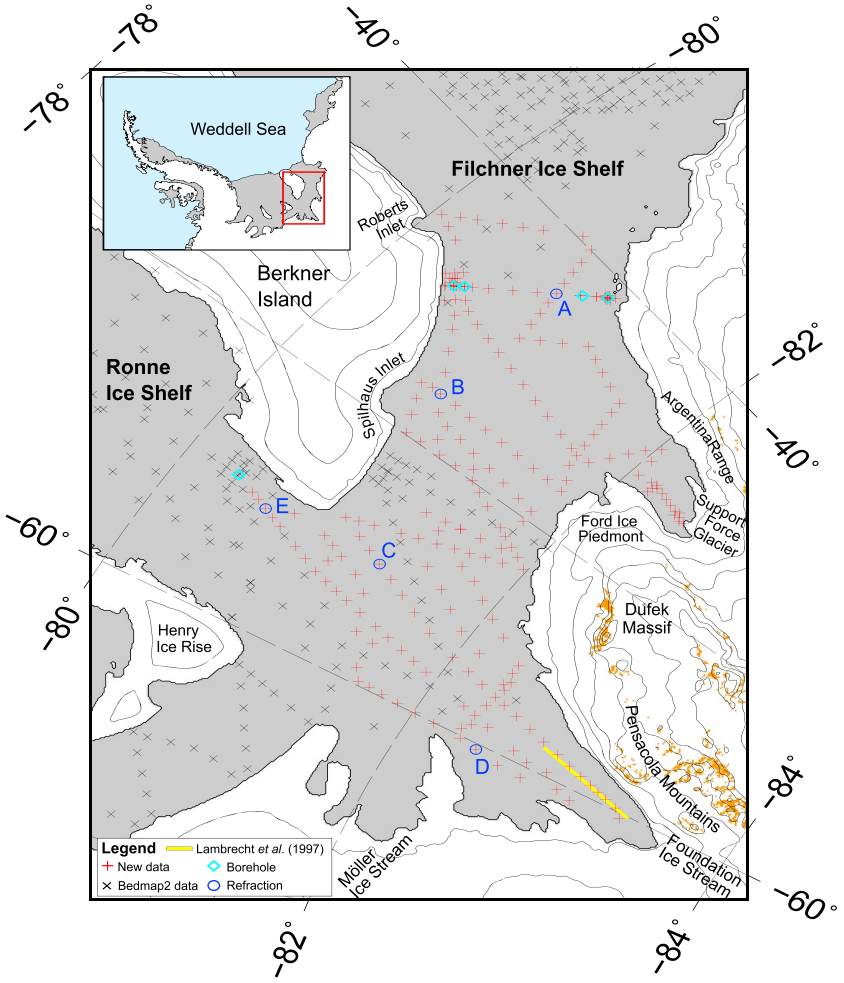

Figure 1. Map of the study area, showing new seismic measurements (red crosses), seismic measurements included in Bedmap2 (black crosses), and seismic measurements previously made near Foundation Ice Stream (yellow line). Also shown are the locations of sub-ice shelf borehole sites (cyan diamonds) and refraction experiments (blue circles). Ice shelf is colored gray and grounded ice is given in white, with 200-m surface height contours in black lines and rock outcrops in yellow (all from Bedmap2).

an important part of the global thermohaline circulation. In addition, many of the largest ice streams of the marine-based West AIS drain into the FRIS. Although its importance has led to considerable effort going into studying the FRIS, its size and remoteness mean that measurement coverage remains sparse.

The highest rates of ice shelf thinning around Antarctica currently occur where relatively warm ocean waters have access to the ice shelves' bases, often via deep troughs (Paolo et al., 2015; Pritchard et al., 2012; Shepherd et al., 2004). Although currently a "cold cavity" ice shelf, recent model simulations have revealed that the FRIS might be vulnerable to intrusions of relatively warm water into the Filchner Trough (Hellmer et al., 2012; Timmermann & Hellmer, 2013), leading to accelerated sea level rise (Thoma et al., 2015). A key uncertainty in model simulations of this kind results from the uncertainty in the shape of the ocean cavity beneath the ice shelf. Deep troughs play a critical role in providing access to the ice shelf base far from the ice front and the interactions of tidal currents (which are generally strong beneath FRIS) with topography have important effects on the melt rate distributions (Mueller et al., 2018). Airborne radar can provide detailed maps of ice thickness but cannot penetrate the water cavity beneath ice shelves to measure its geometry. Inverting for water column thickness from gravity measurements is a possible approach but one that is sensitive to assumptions about the local geological properties (Brisbourne et al., 2014). Although labor intensive, seismic techniques remain the only reliable and direct way to measure ice shelf cavity geometry far from their open ocean boundaries.

This paper presents results from several recent seismic surveys of the southeastern FRIS (Figure 1). This area was targeted because prior to this study it had some of the sparsest data coverage of the major Antarctic ice shelves. Furthermore, current theories on the circulation beneath the FRIS suggest that water flows through this area between the Filchner and Ronne portions of the FRIS, connecting them thermally and acting as a conduit for increased ocean heat transport toward the deep grounding lines under climate change (Timmermann & Goeller, 2017). Combining our new results with existing data in the region, we produce a grid of the sub-ice shelf bathymetry and water column thickness, revealing new features that help enhance our understanding of the ocean circulation and paleo-ice stream flow in this area and providing a more accurate framework for ice-ocean modeling of the FRIS.

2. Data and Methods

2.1. Data Acquisition

The data were collected over the course of three seasons by a number of field parties, consisting of two main surveys during the 15/16 and 16/17 austral summers and several smaller surveys, as part of a joint initiative between the British Antarctic Survey (BAS) and the Alfred Wegener Institute in the framework of the "Filchner Ice Shelf System" and the "Filchner Ice Shelf Project." A total of 256 point seismic measurements were made, of which 248 had clearly visible reflections and were deemed usable. In addition to the standard seismic recordings used to determine ice and water column thickness, 22 refraction measurements were made at five sites across the region to better constrain seismic velocities in the firn (Figure 1). For the bulk of measurements (~85%), acquired during the two main surveys, acquisition methodology was kept consistent.

A powered auger was used to drill shot holes of ~5-m depth, which were then loaded with 150–300 g of high explosives. From each shot hole, a line of 24 receivers were buried to a shallow and consistent depth to ensure good coupling with the snow and reduce wind noise. Receivers were spaced at 10-m intervals, with the first receiver offset from the shot hole by 30 m. The shot hole was backfilled, and a seismic timer was used to detonate the explosives and simultaneously trigger the seismograph. A 24-channel Geometrics Geode data logger was used with a 0.25-ms sampling interval and total record length of 4,096 ms. An example recording is shown in Figure 2a.

The remaining (~15%) measurements were acquired using a hammer-seismics approach, whereby a plate was struck with a ~7-kg sledgehammer, acting as seismic source and also initiating the seismograph recording using a piezoelectric trigger. In order to compensate for the reduced source strength, 5–15 recordings were made at each location and subsequently stacked to improve the signal-to-noise ratio. Apart from the difference in seismic source, these sites used the same methodology as the main surveys.

Seismic reflection quality was generally good except in a few heavily crevassed areas. For the vast majority of seismic records, the seabed reflection was clearly visible in the raw data (Figure 2). At some sites, a frequency-wave number filter was used to reduce ground roll noise and help identify reflections with more certainty. In even fewer cases an automatic gain control filter was also used to reveal the ice base multiple in order to further clarify ambiguous reflections. Wherever possible, the picking was done from the raw data even if a filter was used to help identify reflections, since filtering can lead to a phase shift in the arrival times. At five sites it was not possible to unambiguously identify ice and water base reflections even after filtering, and these points were not included in the final data set.

2.2. Seismic Velocities in Ice and Water

Values for seismic velocity in ice and water are needed in order to convert measured arrival times to ice and water column thicknesses. Boreholes have been drilled at five sites in the region (cyan diamonds in Figure 1) in order to access the sub-ice shelf cavity. Vertical conductivity, temperature, and depth profiles from the ice base to just above the seabed were undertaken at each of these sites, and these data were converted to depth-averaged seismic velocity of the water column. The seismic velocity derived in this manner varied from 1,452.39 to 1,454.70 m/s and for each point in the bathymetric survey the value from the closest site was used to derive water column thickness.

Five shallow refraction surveys were conducted throughout the study region (blue circles in Figure 1) in order to determine seismic velocity within the top 100 m of the ice shelf. At each of the refraction sites, a series of shallow surface shots were carried out, with receiver spacing gradually increasing, from 2.5 to 920 m offset.

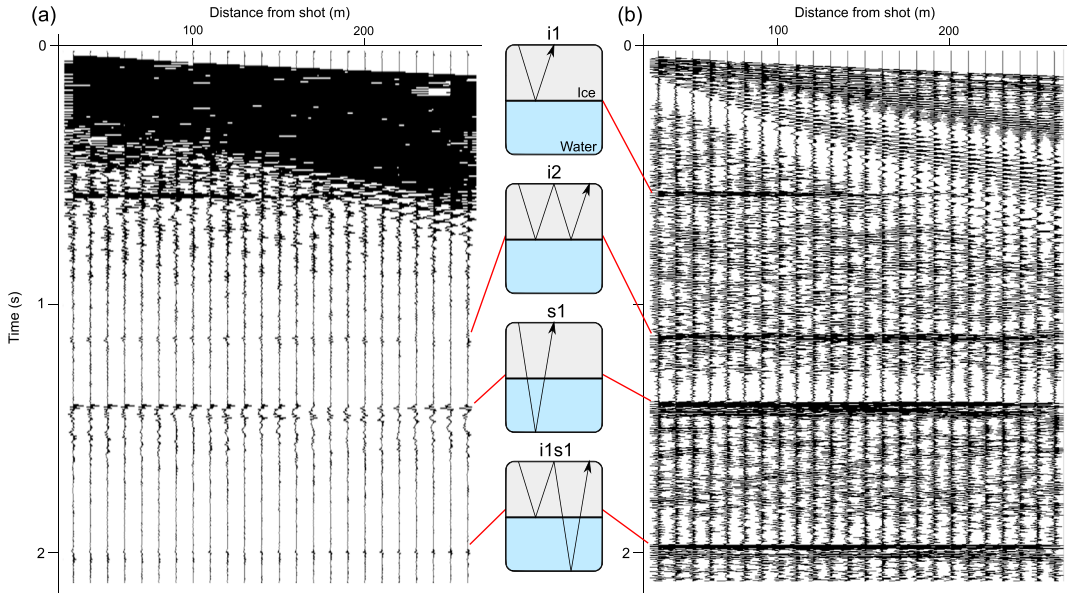

Figure 2. Example of a seismic reflection record (panel a), compared with the same record with an automatic gain control filter applied to enhance weaker returns (panel b). The interpretation for each clear reflection is shown between the two panels (i1: first ice base arrival, i2: ice base multiple, s1: seabed arrival).

The traveltimes of the first arrival at each receiver were then used to obtain a velocity-depth profile (supporting information Figure S1), using the method described by Kirchner and Bentley (1990), which assumes that seismic velocity increases monotonically with depth. Large amounts of surface melting might compromise this assumption by generating layers of ice with different seismic velocity. Thick layers would be visible as discontinuities in traveltime at successive receivers, but given that the traveltime at all sites is smooth and continuous (Figure S1) and that estimates of summer melting in this region are very low (Trusel et al., 2012), the assumption is reasonable.

The resulting correction to surface seismic velocity from the nearest borehole was used at each of the 248 measurement sites. An additional correction was made to compensate for the shot hole depth, using the seismic velocity profile described above and the recorded depth (typically ~5 m).

The refraction approach outlined above provides seismic velocity in the upper 100 m of ice. Below this depth, we assume that ice density is constant and so seismic velocity will depend on ice temperature. Measurements of ice temperature were made through a borehole near site E (marked in Figure 1). Ice temperature at a depth of 100 m was −28°C and remained around this value to within ~150 m of the ice base, at which point the ice temperature increases with depth, reaching −2.6°C at the base of the shelf. Similar temperatures at approximately 100-m depth were also observed at the borehole sites marked with cyan diamonds in Figure 1. Using the temperature-velocity relation of Kohnen (1974) yields a depth-averaged seismic velocity below the top 100 m of 3,861 m/s.

Since the ice thickness at borehole E (~762 m) is similar to the mean thickness of the shelf across all sites (~840 m) we assume that this temperature is broadly representative of ice temperatures below 100 m for the entire region. The assumption that ice temperature varies linearly from 100-m depth to the ice base (e.g., Brisbourne et al., 2014; Johnson & Smith, 1997; Nost, 2004; Smith & Doake, 1994) is clearly not appropriate in this region and would result in average velocity in ice of 3,825 m/s. Regardless, an uncertainty of ±20 m/s introduces an error of ±0.5%, which is small compared with other sources. We use the average seismic velocity described above, together with the surface correction from the nearest refraction site, to convert traveltimes to ice thickness. Spatial variability in seismic velocity, arising from variation in surface ice properties as determined by the refraction experiments, is very small (Figure S1b).

2.3. Uncertainties

There are three main sources of uncertainty in the estimates of ice and water column thickness: uncertainty in picking of reflections, uncertainty in the seismic velocity of ice and water, and uncertainty in the shape of the seabed and ice base. We attempt to quantify these uncertainties in order to provide error estimates for ice and water column thickness at each site.

Picking of ice and seabed reflections was repeated on three separate occasions for each site in order to help quantify the error. For the vast majority of sites, determining the timing of the first arrival for each reflection was possible to within 0.5 ms (approximately equivalent to thickness uncertainties of 0.7 and 1.9 m for water and ice, respectively). At a few sites, particularly near the Foundation Ice Stream (FIS) grounding line, the first arrival was less sharp and so the picking error was greater. The picking error, as determined by repeatability and ambiguity of the first arrival, was estimated for each reflection at each site and contributes to the final error estimate.

Uncertainty in the seismic velocity of ice is discussed in section 2.2. A conservative estimate is that our assumptions lead to an error of $\pm$20 m/s in seismic velocity, corresponding to an error in ice thickness of $\pm$10 m for typical ice thicknesses in the region. Seismic velocity in seawater is better constrained and shows less spatial variability. The spread of seismic velocities measured by conductivity, temperature, and depth profiles would suggest a possible uncertainty of $\pm$2 m/s, less than 0.2% of the mean value. This corresponds to an error of up to $\pm$2 m depending on the total water column thickness.

A final potential source of uncertainty is in the shape of the ice base and seabed (Nost, 2004). Our calculations of ice and water column thickness from traveltimes assume that the ice-water and water-bed interfaces are horizontal and planar. Where this is the case and given a seismic velocity, a characteristic parabola can be fitted to the normal moveout (NMO) deviation of the traveltime along the receiver array. Deviation from the NMO, which would be indicative of a sloping interface, was measured as the time difference between the arrival time at the last receiver and the expected arrival time for a horizontal and planar reflector. Large slopes on the base of floating ice would be unexpected and indeed the largest NMO deviation was 2 ms across the entire region. In general, NMO deviation for the seabed was also small; 93% of sites had an NMO deviation of less than 5 ms, and only three sites had an NMO deviation of greater than 10 ms. A proper assessment of the interface geometry would require multiple shots at different angles across the slope, and this was not done; however, the NMO deviations at the vast majority of sites are sufficiently small that the seabed slope and hence water column thickness error will be small (<10 m, Brisbourne et al., 2014).

2.4. Gridding

The main result of the seismic surveys described above, combined with estimates of seismic velocity, is a collection of 248 new point measurements of ice and water column thickness. Existing seismic data in the region consists largely of data that are included in Bedmap2, arising from a number of previous surveys (230 points, black crosses in Figure 1, Behrendt et al., 1974; Johnson & Smith, 1997; Lythe & Vaughan, 2001; Mayer et al., 1995; Pozdeev & Kurinin, 1987; Vaughan et al., 1995), together with a closely spaced line of seismic measurements near FIS that has not been previously included in any grid of sub-ice shelf topography (106 points, cyan dots in Figure 1; Lambrecht et al., 1997).

Ice shelf geometry can be defined most simply by three measurements: surface elevation, ice thickness, and bed topography. Our strategy for producing a new regional digital elevation model was to focus entirely on bed topography beneath the ice shelf. Everywhere in the grid domain, ice thickness, and surface elevation are set equal to Bedmap2. On grounded ice, and along a 10-km boundary around the domain, bed topography is also the same as in Bedmap2. This results in a seamless transition between the old Bedmap2 grid and this new regional grid and no change in the grounding line position from Bedmap2, which is well constrained by a combination of Moderate Resolution Imaging Spectroradiometer imagery and synthetic aperture radar interferometry (Fretwell et al., 2013). One consequence of this approach is a slight inconsistency, since we use our seismic-derived ice thickness measurements to give sub-ice shelf bathymetry at each point but use Bedmap2 ice thickness when producing the grid of water column thickness. This was done to avoid regridding Bedmap2 ice thickness, which would further complicate any comparison, and the resulting mismatch between the two ice thicknesses is generally small (Figure S2). This only affects our map of water column thickness, since that is the only stage at which we use the Bedmap2 ice thickness grid.

Each of the 587 point measurements of ice and water column thickness can be converted to bed topography, given the surface elevation. These points are then combined with the bed topography on grounded ice and around the edge of the domain and gridded using the ArcGIS Topogrid algorithm (Hutchinson, 1988). Considerable effort went into validating this gridding algorithm for use in Bedmap2 (Fretwell et al., 2013), and, although various algorithms were tested on this data set, we do not repeat that discussion here. The mean distance between seismic measurements on the ice shelf in this new combined data set is 6 km, and all the major features that we discuss herein are robust, that is, not dependent on any particular choice of gridding algorithm.

3. Results and Discussion

A map of seabed elevation in the region, resulting from gridding all available seismic data as described in section 2.4, is shown in Figure 3. In order to aid our discussion, we highlight areas of particular interest where the vast majority of data are new (panels b–d) and compare these with bed topography from Bedmap2 (outlined in red in each panel). We make a comparison with Bedmap2 because this remains the most widely used and up-to-date grid of sub-ice shelf bathymetry beneath the FRIS. Our aim in making the comparison is not to show the inaccuracies in Bedmap2; given the previously poor coverage in our study area these are unsurprising. Rather, the comparison helps interpretation of the new bathymetry by highlighting features that have been missed previously and will undoubtedly affect oceanographic and glaciological processes in the region. An equivalent map of water column thickness is shown in Figure 4 and transects across noteworthy features (whose locations are identified in Figure 3) are shown in Figure 5.

3.1. Implications for Ocean Circulation and Sub-Ice Shelf Melt Rates

Over continental shelves the details of the ocean circulation are strongly dependent on local topography. The seafloor topography helps determine the flow of dense gravity currents; the water column thickness distribution guides barotropic flows; and, in sub-ice shelf cavities, the ice-base topography largely determines the flow of buoyant gravity currents.

The ocean circulation beneath FRIS has been described by Nicholls et al. (2009) with a revision to the pattern beneath the northern Filchner Ice Shelf presented by Darelius et al. (2014). Broadly, dense water is produced north of the Ronne Ice Shelf Front by intense sea ice formation, resulting in a flow of water at the surface freezing point into the sub-ice shelf cavity, along the downward-sloping seafloor. This is the water that supplies the heat for melting at the ice shelf's base. The water circulates anticyclonically around Berkner Island, to exit the cavity, chilled and slightly freshened, at the Filchner Ice Shelf Front.

South of Berkner Island, the bathymetry in Bedmap2 was based on very sparse data coverage, and the interpretation of available sub-ice shelf oceanographic data (e.g., Nicholls et al., 2001; Nicholls & Osterhus, 2004) was heavily caveated as a result. Similarly, the results of ocean models had to be interpreted with caution in this region, although models with spatial resolutions high enough to be significantly affected by the lack of reliable topographic data are only now being applied (e.g., Mueller et al., 2018).

From the main panel in Figure 3, the most obvious feature in the new bathymetry is a sill running across the channel from the southeastern coast of Berkner Island to the mainland, shown in more detail in panel c. This feature exists in a much weaker form in the Bedmap2 grid, although with no supporting data. The map of water column thickness in Figure 4 reveals that the sill results in a narrowing of the sub-ice shelf cavity, which is as little as 200 m thick. Transects across and along the sill in Figure 5 (panels a and b) show its prominence compared with the Bedmap2 grid.

The sill borders a deep depression north of FIS that can potentially capture dense water flowing from the Ronne Ice Shelf Front. Water flowing eastward at depths greater than the sill, around the southern tip of Berkner Island, would be expected to be diverted southward by the sill, across the channel, and then enter a cyclonic circulation within the depression. This is the water that then provides heat for melting the deep Foundation grounding line. The water in the depression would only escape to the east, via the Filchner Ice Shelf cavity, when it had been freshened sufficiently by mixing with meltwater to become less dense and thus to be able to clear the sill's top.

Figure 3b shows the topography of the depression west of the sill in more detail, suggesting a more meandering route for the very deepest water flowing southward from the Ronne Ice Shelf Front. The water column thickness also indicates that this is the likely trajectory for the barotropic component of flow (Figure 4).

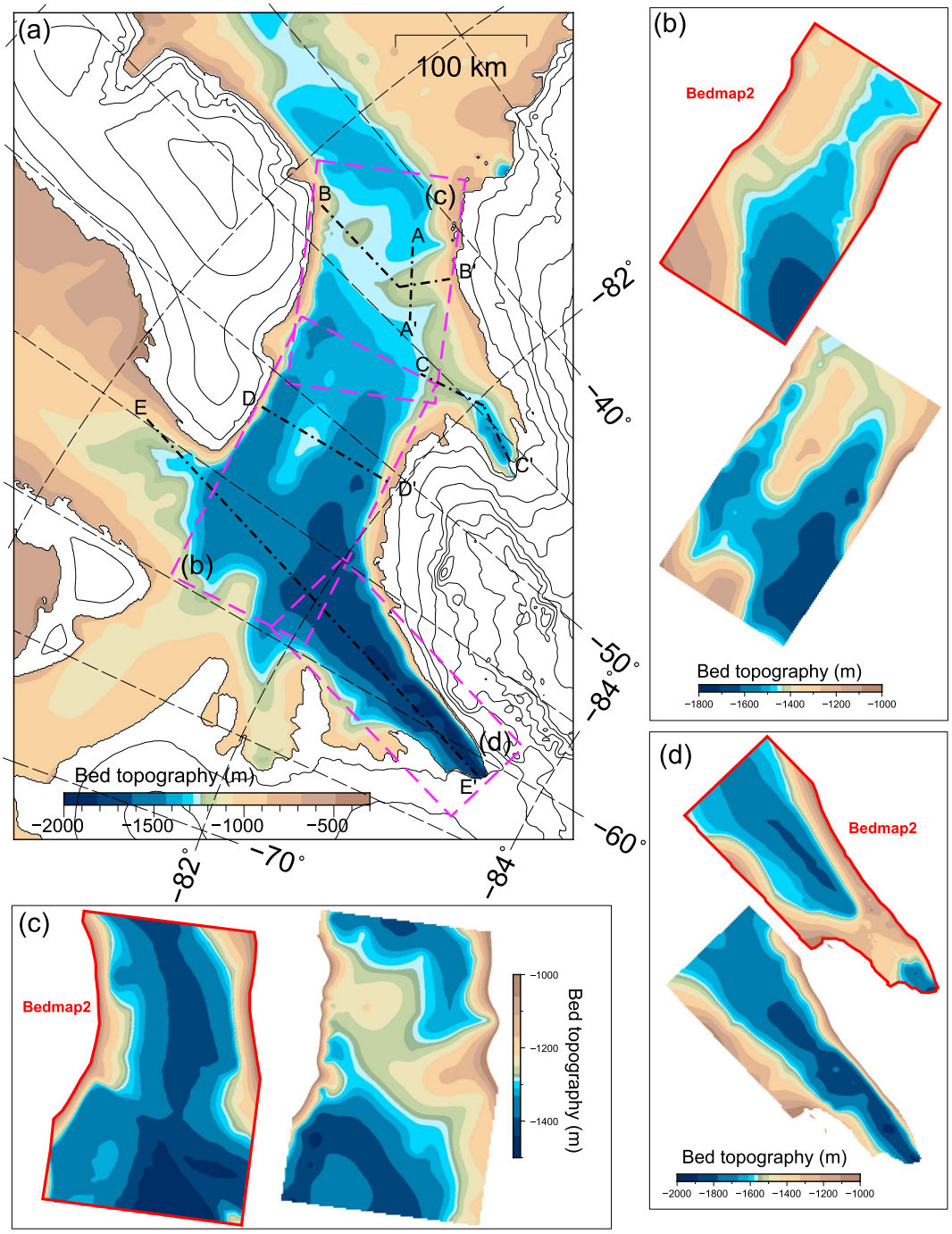

Figure 3. Map of gridded sub-ice shelf bathymetry (panel a). Solid black lines are 200-m ice surface contours from Bedmap2, and dot-dashed lines show the path of the five transects shown in Figure 5. Areas of interest (panels b–d), whose extents are outlined in magenta in panel a, are compared with bed topography from Bedmap2 (outlined in red). Note that different color scales are used in each panel.

A high in the seabed topography, clearly visible in Figure 3b, was poorly resolved and less prominent in Bedmap2 (outlined in red, same panel). It rises steeply on all but its eastern flank, with an elevation change of almost 400 m to the south, and 300 m to the north and west. A transect across its shallowest point is shown in Figure 5d.

Three major ice streams flow into the study region: Möller Ice Stream, FIS, and Support Force Glacier (Figure 1). Of these, FIS is by far the largest, with an ice flux of 33 Gt/year, making it the third largest ice stream feeding

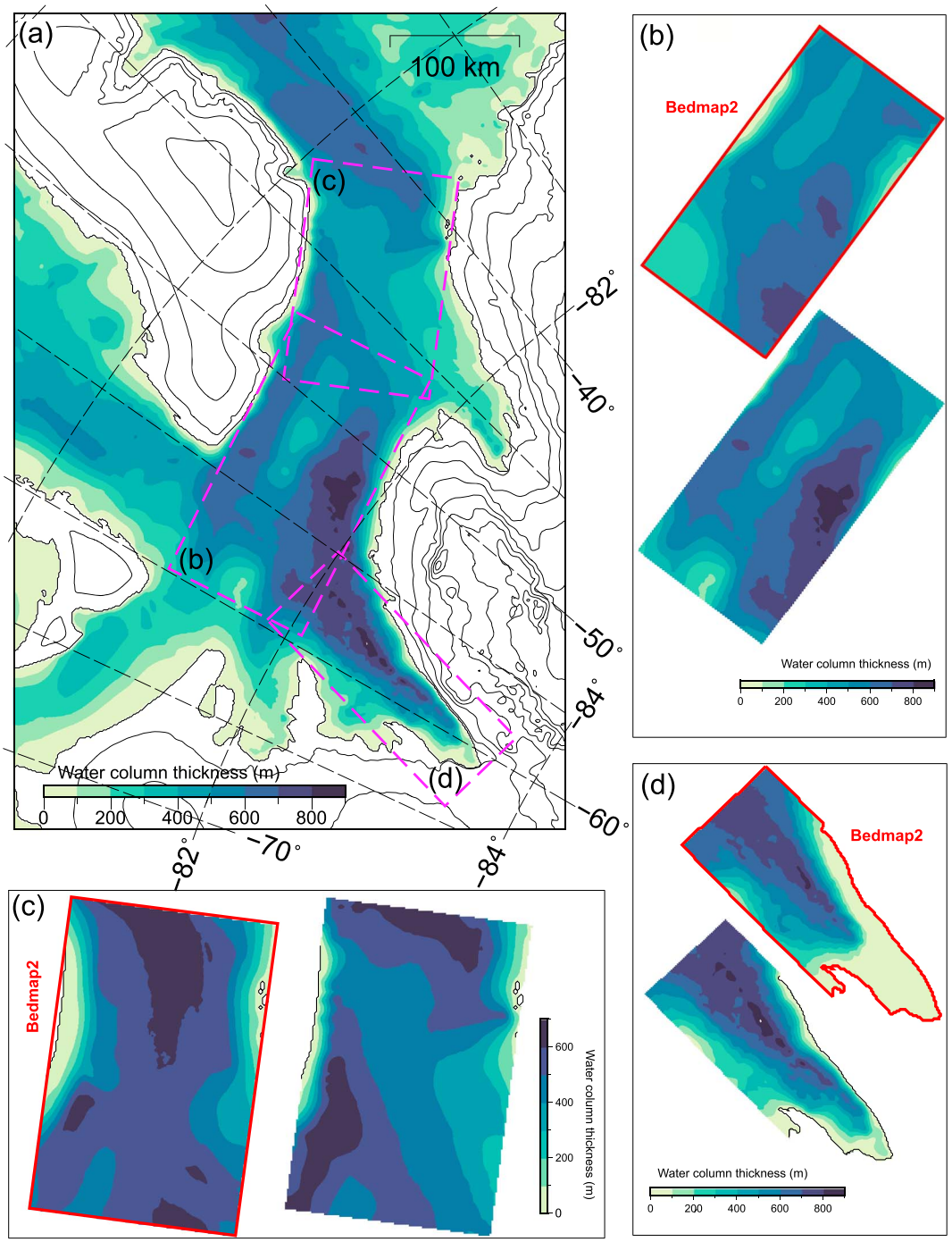

Figure 4. Map of water column thickness, calculated using sub-ice shelf bathymetry from the new grid, together with ice thickness and surface elevation from Bedmap2 (panel a). Solid black lines are 200-m ice surface contours from Bedmap2. Areas of interest (panels b–d) are compared with bed topography from Bedmap2 (outlined in red). Note that different color scales are used in each panel.

into the FRIS by this metric, and the second largest by catchment area (Joughin & Bamber, 2005). A recent study has highlighted the vulnerability of FIS to ice shelf thinning due to loss of buttressing (Reese et al., 2018). At the same time, Mueller et al. (2018) showed that the melting response to ocean warming at FIS strongly depends on the cavity shape, highlighting the importance of accurate bathymetry data for future predictions, which are particularly pertinent in this area. Indeed, melt rates in excess of 5 m/a are currently estimated along

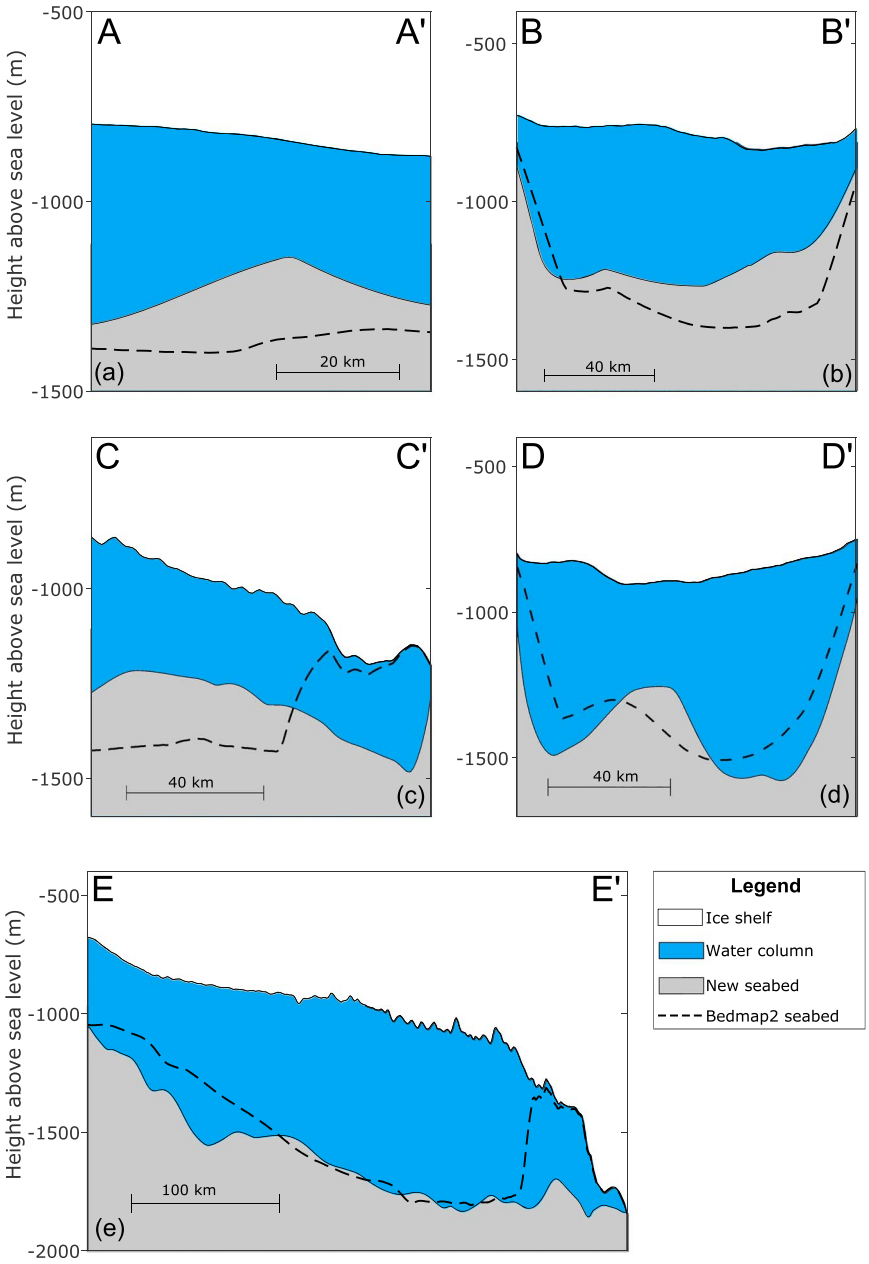

Figure 5. Transects of seabed elevation across the new bathymetric grid (gray shading), together with ice shelf draft (white shading), water column (blue shading), and Bedmap2 seabed elevation (dashed line). The locations of the various transects are shown in Figure 3.

the outflow of FIS (Moholdt et al., 2014), suggesting that considerable heat is available in this portion of the ice shelf cavity.

A deep elongate trough just in front of the FIS grounding line is confirmed by our new data as being continuous, whereas in the Bedmap2 grid it is interrupted by a marked sill (Figures 3d and 5e), with a rather small water column thickness near the grounding line (likely an artifact of the gridding). From an oceanographic point of view, the absence of a sill implies an absence of any topographic barrier to dense, relatively warm water coming into contact with the deep grounding line of FIS. This explains the relatively high melt rates that already exist in the area but also raises the possibility of increased melting in the future.

The bathymetry in front of Support Force Glacier was completely unknown prior to this study but is now captured relatively well (Figure 1). At the grounding line, a deep basin is present but continues only a short

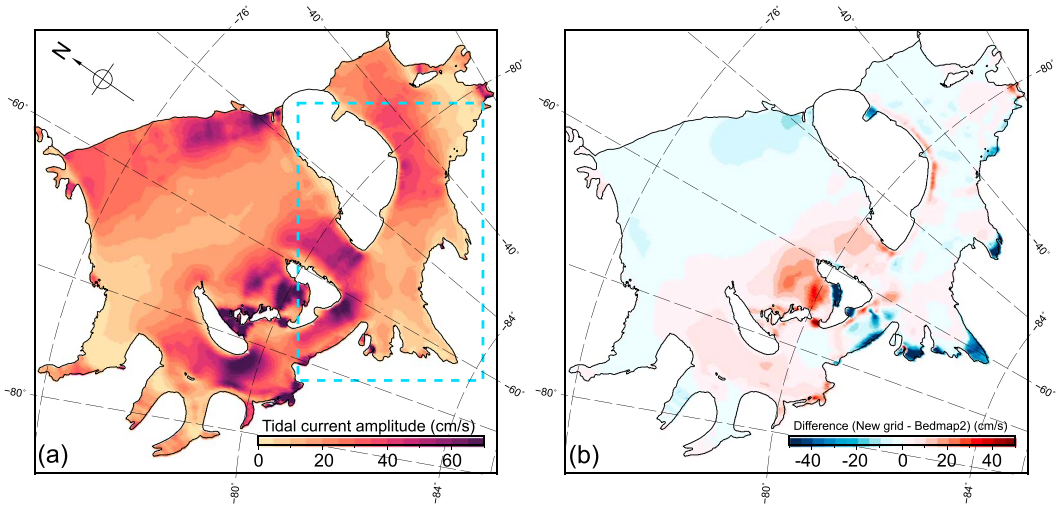

Figure 6. Model results showing the sum of the major axis tidal current velocities for the four main constituents (M_2, S_2, N_2, and K_1) using the new bathymetry (panel a) and the difference in this value for the same model run using the Bedmap2 bathymetry (panel b). The spatial extent of the area covered by the new grid is outlined in cyan.

distance before encountering a small sill (Figure 5c). This would suggest that Support Force Glacier is less vulnerable to oceanic melting compared with FIS.

3.2. Ocean Tidal Modeling

Ocean tides can have a significant impact on circulation and melting/refreezing beneath an ice shelf cavity by increasing turbulence (and thus mixing) close to the ice base. Beneath the FRIS, which is subjected to the largest tides in Antarctica (Padman et al., 2002, 2018), including tides in an ocean model can greatly increase melting and refreezing rates (Makinson et al., 2011; Mueller et al., 2018). The interaction of tidal currents with topography is also found to play an important role in modulating the melting response to potential ocean warming, with local and nonlocal feedbacks as a response to a changing cavity shape (Mueller et al., 2018). Hence, the new bathymetry presented here will likely lead to large changes in tidal currents beneath the FRIS.

To explore how the new bathymetry presented herein might alter tidal currents, the Finite Volume Community Ocean Model (described in Appendix A) was run with both the new and the original Bedmap2 bathymetry in a two-dimensional tidal configuration. Figure 6 shows the sum of the major axis tidal current velocities for the four main constituents (M_2, S_2, N_2, and K_1) for the new bathymetry (panel a), together with the difference between the tidal current amplitudes for the new bathymetry and Bedmap2 (panel b). The largest differences include a reduction in tidal current velocity resulting from an increase in water column thickness near major ice stream grounding lines in the new grid domain, which is found to have large consequences for basal melting (not included in our model) in those regions (Mueller et al., 2018). Similar sensitivities were found by Padman et al. (2018), who showed that tidal amplitudes near the grounding lines of the southwestern Ronne Ice Shelf were greatly improved when applying a deeper and more realistic bathymetry in the fjords. Interestingly, large differences in tidal currents are also found outside of the area of modified bathymetry (outlined in cyan in Figure 6a), highlighting the nonlocal effects of bathymetry variations.

Comparing the simulations with observed tidal currents at six borehole locations on the Filchner and eastern Ronne Ice shelves (not shown), the root-mean-square error is slightly improved with the new bathymetry (6.28 cm/s, as against 6.66 cm/s using the Bedmap2 bathymetry). In particular, the increase in tidal velocities along the western Filchner Trough matches well with the observations, whereas increased velocities at the southwestern tip of Berkner Island lead to a poorer fit at that site (borehole E in Figure 1). While the fit could probably be improved by further tuning, a possible explanation is that the boundary conditions for our forward model were taken from a tidal assimilation that employs the original bathymetry (Padman et al., 2002) and may match less well with the new geometry. The significant reduction in water column thickness at the newly mapped sill across the channel near the southern tip of Berkner Island is likely to affect the tidal Kelvin waves that propagate from the Ronne into the Filchner cavity (Makinson & Nicholls, 1999; Nicholls et al., 2009), causing differences in tidal resonance.

3.3. Implications for Glacial History

Our improved bathymetric grid can also provide insights into the glacial history of the Weddell Sea Embayment and in this context the sill between Berkner Island and the mainland (Figure 3c) is of particular interest. Ice sheet models (e.g., Golledge et al., 2012; le Brocq et al., 2011) and marine geological reconstructions (Larter et al., 2012) suggest that at the Last Glacial Maximum (LGM; approximately 19–25 ka before present [B.P.]) FIS, and possibly even Moller and Institute ice streams (Siegert et al., 2013), which all feed into the Ronne Ice Shelf today, drained into a grounded ice stream flowing through Filchner Trough across the continental shelf. The advance of the Filchner paleo-ice stream onto the outer continental shelf is documented by the presence of subglacial bedforms and sediments on the seabed (Hillenbrand et al., 2012, 2014; Larter et al., 2012; Stolldorf et al., 2012) but seems to be at odds with terrestrial geological reconstructions indicating only very limited ice sheet thickening in the Ellsworth and Shackleton Mountains at the LGM (Bentley et al., 2010; Hein et al., 2011). Whitehouse et al. (2017) recently published a numerical flow line modeling study constrained by new data on LGM ice sheet thickness and post-LGM ice sheet thinning adjacent to FIS (Balco et al., 2016; Bentley et al., 2017) and Bedmap2 bathymetric data. The model experiments identified two alternative stable LGM grounding line positions for the Filchner paleo-ice stream: One position coincides with the continental shelf edge, and the other position is located on a small bathymetric high level with the northern margin of Berkner Island, which was not overridden by inland ice at the LGM (Mulvaney et al., 2007).

We suggest that the prominent bathymetric high identified in our study formed an important pinning point where the grounding line of the Filchner paleo-ice stream halted for some time during post-LGM retreat. In contrast, it is unlikely that the shallow marks the LGM grounding line position. This is because new subglacial bedform and chronological data collected from the outer shelf part of Filchner Trough show that the grounding line was located there until after 11.8 ka B.P. and retreated onto the inner shelf before 8.7 ka B.P. (Arndt et al., 2017), possibly to the bathymetric sill NE of today's Support Force Glacier grounding line. Subsequent retreat from this pinning point probably coincided with a period of maximum ice sheet thinning between 8.9 and 5.2 ka recorded adjacent to FIS (Balco et al., 2016; Bentley et al., 2017).

4. Conclusions

We have presented the results of a bathymetric survey of the southeastern FRIS. The bathymetry in this portion of the ice shelf has, until now, been very poorly constrained. Using the ice surface and thickness products from Bedmap2 and collating all new and previous measurements of sub-ice shelf bathymetry in the area has allowed us to produce new maps of bed topography and water column thickness.

A comparison between the new grid of sub-ice shelf bathymetry and the widely used Bedmap2 product reveals several features that were previously either undersampled or missing altogether. In particular, the presence of a sill between Berkner Island and the Antarctic mainland has important implications for the exchange of water between the Ronne and Filchner ice shelf cavities, potentially forming a barrier preventing the deepest water from flowing eastward until it has been sufficiently freshened by mixing with meltwater. The sill also has implications for our understanding of the development of the Filchner paleo-ice stream, and incorporating our new bathymetric data into flow line models may lead to further insights into its post-LGM retreat history and dynamics. At the outlet of FIS, a sill previously present in bathymetric grids has been confirmed as a gridding artefact. The trough emerging from the grounding line continues northward uninterrupted, allowing relatively warm water to access the deepest parts of the ice shelf where it has a high melting potential.

Ocean tides are highly sensitive to bathymetry and changes in turbulent mixing within the ice shelf cavity could lead to large changes in melting and refreezing rates. A regional ocean model found large differences in tidal current velocities within the entire FRIS cavity arising from changes in bathymetry within the gridded region, as compared with Bedmap2. The model shows that accurate local topography is important for tidal effects on melting near the deep grounding lines but also alters the tidal resonance of the cavity as a whole.

The FRIS and the ocean cavity beneath it form an important and complex part of the climate system. Accurate bathymetric data are essential for improving models of the ice-ocean interactions in this area. The increasingly high spatial resolution used in ocean models beneath ice shelves means that the availability of high-quality bathymetric grids is becoming more and more important. The greatly improved coverage in this area will not only help enhance our understanding of the present-day oceanography beneath the ice shelf but also allow for improved predictions of mass loss from the AIS in its Weddell Sea sector and thus better projections of global sea level rise in the future.

Appendix A: Ocean Model Description

Simulations of barotropic (two-dimensional) tidal currents for the new and Bedmap2 cavity geometries were performed using the Finite Volume Community Ocean Model (Chen et al., 2003), which solves the prognostic free-surface primitive equations for momentum and continuity on a triangular unstructured grid in the horizontal direction and employs a terrain following vertical coordinate that is augmented to include a freely floating ice shelf geometry. The common problem of terrain-following coordinate models in representing steeply sloping topography is absent in the two-dimensional configuration, such that the model is run with the unsmoothed topographic fields, including a vertical ice front and a minimum water column thickness near the grounding lines of a few meters, which can be maintained under larger tidal amplitudes by employing a wetting and drying scheme, although wetting beyond the prescribed grounding lines is not permitted.

The regional configuration covers the FRIS cavity and adjacent continental shelf, with an open boundary that extends into the deep Weddell Sea, crossing the shelf break at 17° W and 53° W, respectively. The horizontal grid spacing varies from 800 m in the Filchner Trough region from the continental shelf break and into the Filchner cavity to 1.5 km over the greater vicinity of Berkner Island (approximate radius of 250 km) and to 3 km in the remainder of the domain. The model is forced along the open boundary with sea surface elevation changes induced by the major tidal constituents M_2, S_2, N_2, and K_1 that were obtained from an Antarctic tidal assimilation (Padman et al., 2002). A quadratic friction law at the seabed and the ice shelf base and resolution-dependent viscosity are employed for dissipation, as well as a sponge region to minimize spurious reflections at the open boundary. The model is run for a simulation time period of three arbitrary months and the tidal velocities are obtained from harmonic analysis of hourly time series from the last simulation month.

Acknowledgments
We thank A. Lambrecht for providing seismic data near FIS grounding line, P. Fretwell and M. Cooper for their help with Bedmap2 data, and L. Padman for helpful discussions regarding the tidal model results. We are very grateful to BAS logistics, pilots, and field assistants for their tireless work to help acquire the data. We would also like to thank Ralph Timmermann and an anonymous reviewer for their comments that helped improve the manuscript. This work was funded by the UK Natural Environment Research Council large grant "Ice shelves in a warming world: Filchner Ice Shelf System" (NE/L013770/1), the AWI strategic fund, and the Norwegian Research Council project 231549 "Inflow of Warm Deep Water on the Antarctic Continental Shelves." The point seismic data set is publicly available through the UK Polar Data Centre at http://doi.org/10.5285/dada63fb-c40a-4b13-97ba-c53860881d79.

References

Arndt, J., Hillenbrand, C.-D., Grobe, H., Kuhn, G., & Wacker, L. (2017). Evidence for a dynamic grounding-line in outer Filchner Trough, Antarctica, until the early Holocene. *Geology*, *45*, 1035–1038.

Balco, G., Todd, C., Huybers, K., Campbell, S., Vermeulen, M., Hegland, M., et al. (2016). Cosmogenic-nuclide exposure ages from the Pensacola Mountains adjacent to the Foundation Ice Stream, Antarctica. *American Journal of Science*, *316*(6), 542–577. https://doi.org/10.2475/06.2016.02

Behrendt, J. C., Henderson, J. R., Meister, L., & Rambo, W. L. (1974). The temperature dependance of seismic waves in ice. *United States Geological Survey Profession Paper*, *844*, 28.

Bentley, M., Fogwill, C., Le Brocq, A., Hubbard, A., Sugden, D., Dunai, T., & Freeman, S. (2010). Deglacial history of the west Antarctic ice sheet in the Weddell Sea embayment: Constraints on past ice volume change. *Geology*, *38*, 411–414.

Bentley, M., Hein, A., Sugden, D., Whitehouse, P., Shanks, R., Xu, S., & Freeman, S. (2017). Deglacial history of the Pensacola Mountains, Antarctica from glacial geomorphology and cosmogenic nuclide surface exposure dating. *Quaternary Science Reviews*, *158* (Supplement C), 58–76. https://doi.org/10.1016/j.quascirev.2016.09.028

Brisbourne, A. M., Smith, A. M., King, E. C., Nicholls, K. W., Holland, P. R., & Makinson, K. (2014). Seabed topography beneath Larsen C Ice Shelf from seismic soundings. *The Cryosphere*, *8*(1), 1–13. https://doi.org/10.5194/tc-8-1-2014

Chen, C., Liu, H., & Beardsley, R. C. (2003). An unstructured grid, finite-volume, three-dimensional, primitive equations ocean model: Application to coastal ocean and estuaries. *Journal of Atmospheric and Oceanic Technology*, *20*(1), 159–186. https://doi.org/10.1175/1520-0426

Darelius, E., Makinson, K., Daae, K., Fer, I., Holland, P. R., & Nicholls, K. W. (2014). Hydrography and circulation in the Filchner Depression, Weddell Sea, Antarctica. *Journal of Geophysical Research: Oceans*, *119*, 5797–5814. https://doi.org/10.1002/2014JC010225

Dupont, T. K., & Alley, R. B. (2005). Assessment of the importance of ice-shelf buttressing to ice-sheet flow. *Geophysical Research Letters*, *32*, L04503. https://doi.org/10.1029/2004GL022024

Fox, A. J., Paul, A., & Cooper, R. (1994). Measured properties of the Antarctic ice sheet derived from the scar Antarctic digital database. *Polar Record*, *30*(174), 1994. https://doi.org/10.1017/S0032247400024268

Fretwell, P., Pritchard, H. D., Vaughan, D. G., Bamber, J. L., Barrand, N. E., Bell, R., et al. (2013). Bedmap2: Improved ice bed, surface and thickness datasets for Antarctica. *The Cryosphere*, *7*(1), 375–393. https://doi.org/10.5194/tc-7-375-2013

Gardner, A. S., Moholdt, G., Scambos, T., Fahnstock, M., Ligtenberg, S., van den Broeke, M., & Nilsson, J. (2018). Increased West Antarctic and unchanged East Antarctic ice discharge over the last 7 years. *The Cryosphere*, *12*(2), 521–547. https://doi.org/10.5194/tc-12-521-2018

Golledge, N. R., Fogwill, C. J., Mackintosh, A. N., & Buckley, K. M. (2012). Dynamics of the last glacial maximum Antarctic ice-sheet and its response to ocean forcing. *Proceedings of the National Academy of Sciences*, *109*(40), 16,052–16,056. https://doi.org/10.1073/pnas.1205385109

Hein, A. S., Fogwill, C. J., Sugden, D. E., & Xu, S. (2011). Glacial/interglacial ice-stream stability in the Weddell Sea embayment, Antarctica. *Earth and Planetary Science Letters*, *307*(1), 211–221. https://doi.org/10.1016/j.epsl.2011.04.037

Hellmer, H. H., Krauker, F., Timmermann, R., Determann, J., & Rae, J. (2012). Twenty-first-century warming of a large Antarctic ice-shelf cavity by a redirected coastal current. *Nature*, *485*, 225–228. https://doi.org/10.1038/nature11064

Hillenbrand, C.-D., Bentley, M. J., Stolldorf, T. D., Hein, A. S., Kuhn, G., Graham, A., et al. (2014). Reconstruction of changes in the Weddell Sea sector of the Antarctic ice sheet since the Last Glacial Maximum. *Quaternary Science Reviews*, *100* (Supplement C), 111–136. https://doi.org/10.1016/j.quascirev.2013.07.020, reconstruction of Antarctic Ice Sheet Deglaciation (RAISED).

Hillenbrand, C.-D., Melles, M., Kuhn, G., & Larter, R. D. (2012). Marine geological constraints for the grounding-line position of the Antarctic Ice Sheet on the southern Weddell Sea shelf at the Last Glacial Maximum. *Quaternary Science Reviews*, *32*, 25–47. https://doi.org/10.1016/j.quascirev.2011.11.017

Hughes, T. (1973). Is the west Antarctic Ice Sheet disintegrating?*Journal of Geophysical Research*, *78*(33), 7884–7910. https://doi.org/10.1029/JC078i033p07884

Hutchinson, M. F. (1988). *Calculation of hydrologically sound digital elevation models*. Columbus, Ohio: International Geographical Union, Sydney. 117–133.
Johnson, M. R., & Smith, A. M. (1997). Seabed topography under the southern and western Ronne Ice Shelf, derived from seismic surveys. *Antarctic Science*, *2*, 201–208.
Joughin, I., & Bamber, J. L. (2005). Thickening of the ice stream catchments feeding the Filchner-Ronne Ice Shelf, Antarctica. *Geophysical Research Letters*, *32*, L17503. https://doi.org/10.1029/2005GL023844
Kirchner, J. F., & Bentley, C. R. (1990). RIGGS III: Seismic short-refraction studies using an analytical curve- fitting technique. In C. R. Bentley & D. E. Hayes (Eds.), *The Ross Ice Shelf: Glaciology and geophysics* (pp. 109–126). Washington, DC: American Geophysical Union. https://doi.org/10.1029/AR042p0109
Kohnen, H. (1974). The temperature dependance of seismic waves in ice. *Journal of Glaciology*, *13*, 144–147.
Lambrecht, A., Mayer, C., Hempel, L., Nixdorf, U., & Oerter, H. (1997). Glaciological investigations in the grounding line area of the Foundation Ice Stream, Antarctica. *Polarforschung*, *65*, 15–25.
Larter, R. D., Graham, A. G., Hillenbrand, C.-D., Smith, J. A., & Gales, J. A. (2012). Late quaternary grounded ice extent in the Filchner Trough, Weddell Sea, Antarctica: New marine geophysical evidence. *Quaternary Science Reviews*, *53* (Supplement C), 111–122. https://doi.org/10.1016/j.quascirev.2012.08.006
le Brocq, A. M., Bentley, M., Hubbard, A., Fogwill, C., Sugden, D., & Whitehouse, P. (2011). Reconstructing the Last Glacial Maximum ice sheet in the Weddell Sea embayment, Antarctica, using numerical modelling constrained by field evidence. *Quaternary Science Reviews*, *30*(19), 2422–2432. https://doi.org/10.1016/j.quascirev.2011.05.009
Lythe, M. B., & Vaughan, D. G. (2001). BEDMAP: A new ice thickness and subglacial topographic model of Antarctica. *Journal of Geophysical Research*, *106*(B6), 11,335–11,351. https://doi.org/10.1029/2000JB900449
Makinson, K., Holland, P. R., Jenkins, A., Nicholls, K. W., & Holland, D. M. (2011). Influence of tides on melting and freezing beneath Filchner-Ronne Ice Shelf, Antarctica. *Geophysical Research Letters*, *38*, L06601. https://doi.org/10.1029/2010GL046462
Makinson, K., & Nicholls, K. W. (1999). Modeling tidal currents beneath Filchner-Ronne Ice Shelf and on the adjacent continental shelf: Their effect on mixing and transport. *Journal of Geophysical Research*, *104*(C6), 13449–13465. https://doi.org/10.1029/1999JC900008
Mayer, C., Lambrecht, A., & Oerter, H. (1995). *Glaciological investigations on the Foundation Ice Stream*. Bremerhaven: Alfred-Wegener-Institute for Polar and Marine Research. 475–479.
Meredith, M. P. (2013). Replenishing the abyss. *Nature Geoscience*, *6*, 166–167. https://doi.org/10.1038/ngeo1743
Moholdt, G., Padman, L., & Fricker, H. A. (2014). Basal mass budget of ross and Filchner-Ronne ice shelves, Antarctica, derived from Lagrangian analysis of ICESat altimetry. *Journal of Geophysical Research: Earth Surface*, *119*, 2361–2380. https://doi.org/10.1002/2014JF003171
Mueller, R. D., Hattermann, T., Howard, S. L., & Padman, L. (2018). Tidal influences on a future evolution of the Filchner–Ronne Ice Shelf cavity in the Weddell Sea, Antarctica. *The Cryosphere*, *12*(2), 453–476. https://doi.org/10.5194/tc-12-453-2018
Mulvaney, R., Arrowsmith, C., Barnola, J., McCormack, T., Loulergue, L., Raynaud, D., et al. (2007). A deglaciation climate and ice sheet history of the Weddell Sea region from the Berkner Island ice core. *Quaternary International*, *48*, 294–295.
Nicholls, K. W., & Osterhus, S. (2004). Interannual variability and ventilation timescales in the ocean cavity beneath Filchner-Ronne Ice Shelf, Antarctica. *Journal of Geophysical Research*, *109*, C04014. https://doi.org/10.1029/2003JC002149
Nicholls, K. W., Osterhus, S., Makinson, K., Gammerlsrod, T., & Fahrback, E. (2009). Ice-ocean processes over the continental shelf of the southern Weddell Sea, Antarctica: A review. *Reviews of Geophysics*, *47*, RG3003. https://doi.org/10.1029/2007RG000250
Nicholls, K. W., Osterhus, S., Makinson, K., & Johnson, M. R. (2001). Oceanographic conditions south of Berkner Island, beneath Filchner-Ronne Ice Shelf, Antarctica. *Journal of Geophysical Research*, *106*(C6), 11,481–11,492. https://doi.org/10.1029/2000JC000350
Nost, O. A. (2004). Measurements of ice thickness and seabed topography under the Fimbul Ice Shelf, Dronning Maud Land, Antarctica. *Journal of Geophysical Research*, *109*, C10010. https://doi.org/10.1029/2004JC002277
Padman, L., Fricker, H. A., Coleman, R., Howard, S., & Erofeeva, L. (2002). A new tide model for the Antarctic ice shelves and seas. *Annals of Glaciology*, *34*, 247–254. https://doi.org/10.3189/172756402781817752
Padman, L., Siegfried, M. R., & Fricker, H. A. (2018). Ocean tide influences on the Antarctic and Greenland Ice Sheets. *Reviews of Geophysics*, *56*, 142–184. https://doi.org/10.1002/2016RG000546
Paolo, F. S., Fricker, H. A., & Padman, L. (2015). Volume loss from Antarctic ice shelves is accelerating. *Science*, *348*(6232), 327–331. https://doi.org/10.1126/science.aaa0940
Payne, A. J., Vieli, A., Shepherd, A. P., Wingham, D. J., & Rignot, E. (2004). Recent dramatic thinning of largest west Antarctic ice stream triggered by oceans. *Geophysical Research Letters*, *31*, L23401. https://doi.org/10.1029/2004GL021284
Pozdeev, V. S., & Kurinin, R. G. (1987). New data on the morphology of the ice cover and the relief of the subglacial bed and sea bottom in the southern part of the Weddell Sea basin (West Antarctica). *Antarktida, doklady komissii*, *26*, 66–71.
Pritchard, H. D., Ligtenberg, S. R. M., Fricker, H. A., Vaughan, D. G., van den Broeke, M. R., & Padman, L. (2012). Antarctic ice-sheet loss driven by basal melting of ice shelves. *Nature*, *484*, 502–505. https://doi.org/10.1038/nature10968
Reese, R., Gudmundsson, G. H., Levermann, A., & Winkelmann, R. (2018). The far reach of ice-shelf thinning in Antarctica. *Nature Climate Change*, *8*, 53–57. https://doi.org/10.1038/s41558-017-0020-x
Rignot, E., Jacobs, S., Mouginot, J., & Scheuchl, B. (2013). Ice-shelf melting around Antarctic. *Science*, *341*(6143), 266–270. https://doi.org/10.1126/science.1235798
Rott, H., Rack, W., Skvarca, P., & Angelis, H. D. (2002). Northern Larsen Ice Shelf, Antarctica: Further retreat after collapse. *Annals of Glaciology*, *34*, 277–282. https://doi.org/10.3189/172756402781817716
Scambos, T. A., Bohlander, J. A., Shuman, C. A., & Skvarca, P. (2004). Glacier acceleration and thinning after ice shelf collapse in the Larsen B embayment, Antarctica. *Geophysical Research Letters*, *31*, L18402. https://doi.org/10.1029/2004GL020670
Shepherd, A., Wingham, D., & Rignot, E. (2004). Warm ocean is eroding West Antarctic Ice Sheet. *Geophysical Research Letters*, *31*, L23402. https://doi.org/10.1029/2004GL021106
Siegert, M., Ross, N., Corr, H., Kingslake, J., & Hindmarsh, R. (2013). Late holocene ice-flow reconfiguration in the Weddell Sea sector of West Antarctica. *Quaternary Science Reviews*, *78*, 98–107. https://doi.org/10.1016/j.quascirev.2013.08.003
Smith, A. M., & Doake, C. S. M. (1994). Seabed depths at the mouth of Rutford Ice Stream, Antarctica. *Annals of Glaciology*, *20*, 353–356.
Stolldorf, T., Schenke, H.-W., & Anderson, J. B. (2012). LGM ice sheet extent in the Weddell Sea: Evidence for diachronous behavior of Antarctic Ice Sheets. *Quaternary Science Reviews*, *48*(Supplement C), 20–31. https://doi.org/10.1016/j.quascirev.2012.05.017
Thoma, M., Determann, J., Grosfeld, K., Goeller, S., & Hellmer, H. H. (2015). Future sea-level rise due to projected ocean warming beneath the Filchner Ronne Ice Shelf: A coupled model study. *Earth and Planetary Science Letters*, *431*, 217–224. https://doi.org/10.1016/j.epsl.2015.09.013

Thomas, R. H. (1973). The creep of ice shelves: Interpretation of observed behaviour. *Journal of Glaciology*, *12*(64), 55–70. https://doi.org/10.3189/S002214300002270X

Timmermann, R., & Goeller, S. (2017). Response to Filchner–Ronne Ice Shelf cavity warming in a coupled ocean–ice sheet model—Part 1: The ocean perspective. *Ocean Science*, *13*(5), 765–776. https://doi.org/10.5194/os-13-765-2017

Timmermann, R., & Hellmer, H. H. (2013). Southern ocean warming and increased ice shelf basal melting in the twenty-first and twenty-second centuries based on coupled ice-ocean finite-element modelling. *Ocean Dynamics*, *63*(9), 1011–1026. https://doi.org/10.1007/s10236-013-0642-0

Trusel, L. D., Frey, K. E., & Das, S. B. (2012). Antarctic surface melting dynamics: Enhanced perspectives from radar scatterometer data. *Journal of Geophysical Research*, *117*, F02023. https://doi.org/10.1029/2011JF002126

Vaughan, D. G., Sievers, J., Doake, C. S. M., Hinze, H., Mantripp, D. R., Pozdeev, V. S., et al. (1995). Subglacial and seabed topography, ice thickness and water column thickness in the vicinity of Filchner-Ronne-Schelfeis, Antarctica. *Polarforschung*, *64*, 75–88.

Whitehouse, P. L., Bentley, M. J., Vieli, A., Jamieson, S. S. R., Hein, A. S., & Sugden, D. E. (2017). Controls on last glacial maximum ice extent in the Weddell Sea embayment, Antarctica. *Journal of Geophysical Research: Earth Surface*, *122*, 371–397. https://doi.org/10.1002/2016JF00412